

Enhancement of the 1-butanol productivity in the ethanol condensation catalyzed by noble metal nanoparticles supported on Mg-Al mixed oxide

Jorge Quesada, Laura Faba, Eva Díaz, and Salvador Ordóñez*

Department of Chemical and Environmental Engineering, University of Oviedo (Faculty of Chemistry), Julián Clavería s/n, 33006 Oviedo, Spain

*Corresponding Author: E-mail address: sordonez@uniovi.es (S. Ordóñez)

Abstract: The role of the addition of a noble metal (Ru and Pd) on the surface of a basic mixed oxide (MgAl) used as ethanol condensation catalyst is studied in this work. The activity trends for all the reaction steps (dehydrogenation, condensation, dehydration, and hydrogenation) were analyzed, concluding that dehydrogenation step is the rate-determining one under inert conditions whereas hydrogenations also take a relevant role under reducing conditions. Ruthenium has shown very promising 1-butanol productivities at soft conditions (15 times higher than the parent material) whereas palladium performance is limited by the lateral decarbonylation reaction, and its high hydrogenation activity is only determining at temperatures higher than 650 K.

Keywords: Guerbet reaction; butanol; alcohol dehydrogenation; aldol condensation; bifunctional catalyst

1. Introduction

In the general frame of biomass upgrading for obtaining high added-value chemicals, the conversion of ethanol into 1-butanol is getting an increasing attention, with a continuous increase in the number of scientific papers published in this topic (from 432 papers in 2007 to 744 in the past 2017, according to the Web of Science database). Based on the most generally accepted mechanism, this reaction takes place by the Guerbert pathway, involving three tandem reactions: ethanol dehydrogenation, aldol condensation of acetaldehyde and two consecutive hydrogenations of crotonaldehyde. This mechanism is summarized in **Scheme 1**. Most of the scientific efforts have been focused on the development of active catalysts with enough acid and basic sites to enhance the condensation step, typically considered as the most relevant one [1-5]. However, the general conclusion of these studies is that 1-butanol productivity is still far from being competitive, even working over 600 K [6]. This conclusion suggests that the other two steps might also play a key role in the overall butanol yield. If the reaction is catalyzed by an acid-basic sites, dehydrogenation and hydrogenation can also occur, but in a limited extent. C=O hydrogenation is mainly accomplished in the parent catalyst through the Meerwein-Ponndorf-Verley (MPV) reduction, promoting also some dehydrogenation. However, dehydrogenation mainly occurs as a monomolecular mechanism activated by acid-basic sites, releasing some atomic hydrogen that is used for the C=C reduction. At this point, the incorporation of metal nanoparticles supported on an active acid-basic material is reported to improve significantly this yield, because of two concomitant reasons: promoting dehydrogenation steps and increasing hydrogenation activity of the catalysts. According to these premises, the development of a promising catalyst is conditioned by the selection of a noble metal with a good balance between its dehydrogenation and hydrogenation activity [7].

First efforts focused on this strategy are mainly related to transition metals (i.e., Co, Ni, Cu, Fe, etc.), but considering exchange by parent oxide cations or supporting in large amounts [8-12]. These procedures lead to severe changes in the original acidity/basicity of the support, making difficult to identify the real role of the metal. In our previous works, we introduce a different approach, evaluating the effect of including same metals but in very low concentration (in order to affect as less as possible the original acid/basic distribution) and after a reducing pretreatment to have a real idea about their role as metal nanoparticles. Thus, we analyzed the role of cobalt and nickel supported on Mg-Al mixed oxide [13]. This support has a well-known activity for the aldol condensation, being previously proposed as catalyst for this reaction [14-16]. After introducing these metal phases, a clear improvement was obtained working under inert conditions, reaching 1-butanol productivities up to eight times the values obtained with Mg-Al. Best results were obtained with cobalt, metal with the highest dehydrogenation capacity [13]. In a similar set of experiments, a relevant role of reducing atmosphere was also suggested observing an increment in the 1-butanol productivity mainly marked by the decrease in other side reactions related to dehydration and side-dehydrogenation steps (i.e., formation of 1,3-butadiene). However, the limited activity of transition metals for hydrogenation prevents obtaining more evidences. Based on this, the study of other metal more focused on the hydrogenation steps is required in order to obtain a clear and complete understanding about the relative role of each step in the Guerbert reaction.

At this point, this paper proposes the analysis of the activity of two representative noble metals in the ethanol gas-phase condensation: ruthenium and palladium. Palladium nanoparticles based catalysts are widely reported as heterogeneous catalysts for many

transformations, including unsaturated hydrocarbon hydrogenation [17-19]. For cinnamaldehyde hydrogenation, these studies suggest that this metal presents similar activity in the hydrogenation of C=C and C=O bonds [19]. This double hydrogenation capacity is a key point in this reaction, since metals can only hydrogenate the C=C bonds, reaction much more thermodynamically favored [20,21]. These two very different saturations are also present in crotonaldehyde, so a positive effect in the ethanol condensation can be foreseen. In addition, its ability for dehydrogenation [22] and C-C coupling reactions is demonstrated [23]. Considering all these properties, palladium seems to be a good candidate to enhance the 1-butanol productivity.

On the other hand, ruthenium metal centers are known for their ability to reversible perform hydrogen transfer reaction, being useful not only for hydrogenation, but also for the dehydrogenation step [24-27]. As in the case as of palladium, ruthenium shows good activity at hydrogenation involving not only C=C bonds, but also C=O [18]. Thus, a previous study proposes the use of ruthenium as ligand for different organometallic complexes very active as homogeneous catalysts for ethanol condensation, reaching a very high 1-butanol selectivity (94 %) with 20 % of ethanol conversion [6]. However, to the best of our knowledge, there are no references for the use of this metal as reduced supported nanoparticles for the ethanol gas-phase condensation, with only a preliminary study about its role in ethanol condensation in liquid phase [12].

Taking into account this background, we propose the use of 1 wt.% Ru and 1 wt.% Pd supported on Mg-Al mixed oxide, a catalyst with a well-known activity for this reaction [14-16]. In order to disturb as less as possible the original catalytic activity of the mixed oxide, metal loading was limited to 1 wt. %. Metals were reduced and well distributed on the

acid/basic surface of Mg-Al, obtaining a very small and monodispersed nanoparticles (around 1.5 nm). With the general aim of increasing the 1-butanol productivity, the role of these bifunctional materials was analyzed in each step of the process, trying to identify the relative weight of each reaction in the global result. Possible side-reactions as well as the evolution of catalytic surface were also considered, in order to complete a thorough analysis of the experimental results.

2. Experimental Methods

2.1. Catalysts Preparation

Mg-Al mixed oxide (Mg/Al = 3) was obtained by the calcination of the corresponding hydrotalcite, prepared by co-precipitation of the Mg and Al nitrates (Aldrich magnesium nitrate hexahydrate, and Aldrich aluminum nitrate nonahydrate) at low supersaturation and under sonication. The gel was precipitated by increasing the pH to 10 with a NaOH solution (10 %) and it was aged at 353 K for 24 hours. The solid phase was then isolated by centrifugation, washed with deionized water to pH 7 and dried at 383 K for 24 hours, reaching the hydrotalcite. Finally, the mixed oxide was obtained by calcining the hydrotalcite in flowing air, from 293 to 973 K with a temperature rate of $5 \text{ K}\cdot\text{min}^{-1}$, holding this set-point for 5 hours. The detailed procedure is reported in the literature [28].

The Pd/Mg-Al and Ru/Mg-Al (1 wt. % of metal) were synthesized by incipient wetness impregnation of each metal precursor on the support, using tetraaminepalladium (II) nitrate 10 wt % solution in water (Aldrich) and ruthenium (III) nitrosyl nitrate 1.5 wt. % solution in dilute nitric acid (Aldrich) as precursors, respectively. Materials were treated under air flow,

from 293 to 973 K with a temperature ramp of $5 \text{ K}\cdot\text{min}^{-1}$, holding this temperature for 5 h. Samples were reduced in a Micromeritics 2900 TPD/TPR instrument, flowing H_2 -Ar mixture (10 vol % of H_2 ; $20 \text{ mL}\cdot\text{min}^{-1}$) for 3 h at 623 K in the case of Pd/Mg-Al and 723 K for Ru/Mg-Al. These temperatures were chosen according to TPR analyses of the parent materials, as it is explained in the characterization section.

2.2. Catalysts characterization

Morphologic properties were determined by N_2 physisorption at 77 K in a Micromeritics ASAP 2020 using the Brunauer-Emmett-Teller (BET) method to analyze the surface area, and the Barret-Joyner-Halenda (BJH) method to calculate the pore volume and diameter. Temperature-programmed reduction analyses (TPR) were carried out to analyze the oxidation state of the metals in a Micromeritics 2900 TPD/TPR. Calcined samples, 10 mg, were treated under H_2 flow (10 vol. % H_2/Ar) from 298 to 973 K, with a temperature rate of $2.5 \text{ K}\cdot\text{min}^{-1}$.

Surface basicity and acidity were analyzed by temperature-programmed desorption (TPD) using the same instrument as for the TPR analyses. In order to prevent any partial oxidation of these nanoparticles, these analyses were carried out directly after the reducing step, in the same instrument, preventing any contact with air that could modify the surface. With all the materials, 10 mg were pre-treated in He flow and saturated with CO_2 or NH_3 to determine the basicity or acidity, respectively. The evolution of CO_2 and NH_3 signals were followed in a Pfeiffer Vacuum Omnistar Prisma mass spectrometer at increasing temperature, from 298 to 973 K, with a temperature ratio of $2.5 \text{ K}\cdot\text{min}^{-1}$.

The crystallographic structure of the catalysts was determined by X-ray diffraction (XRD) using a Philips PW 1710 diffractometer with a CuK α line (1.54 Å) in the 2 θ range within 5 and 80° at 2°·min⁻¹ of scanning rate. High-resolution transmission electron microscopy (HRTEM) analyses of the fresh materials were carried out to determine the nanoparticle size and distribution, as well as the metal dispersion in a JEOL JEM2100F instrument. Hydrogen chemisorption analyses were also performed in order to determine the metal dispersion and the crystallite size of the used catalysts, obtaining the data using a Micromeritics ASAP 2020.

2.3. Catalytic studies

Activity experiments were carried out in a 0.4 cm i.d. U-shaped fixed bed quartz reactor located inside a controlled electric furnace, studying the evolution of the gas phase (GC-FID, HP6890 Plus) from 523 to 723 K. The catalyst (150 mg; 250-355 μ m) was placed above a quartz wool plug and it was in situ pre-treated at 473 K for 1 h in flowing He-H₂ (10 vol % of H₂) before each experiment. Absolute ethanol was supplied with a syringe pump in the He or H₂-He (10 vol % of H₂) flow (as function on the type of experiment), causing the in situ vaporization, resulting in a 32 vol. % of ethanol, fed to the reactor at 20 mL·min⁻¹ (STP), with 7.9 h⁻¹ value of weight hourly space velocity (WHSV). The product identification was performed using commercial standards and supported by GC-MS (Shimadzu QP-2010).

Conversions (x) were calculated from the ethanol concentrations at the reactor inlet and outlet, whereas carbon balances (CB) were calculated by contrasting the total quantity of carbon atoms at the reactor inlet and outlet, taking into account only the identified products (compounds in **Scheme 1**). Yield (η_i) was calculated as follows:

$$\eta_i (\%) = \left(\frac{\text{C moles in product}}{\text{C moles in ethanol fed}} \right) \cdot 100$$

The productivity (P_i) of the different compounds during the reaction (average formation rate) were determined as follows:

$$P_i (\text{mol} \cdot \text{h}^{-1} \cdot \text{g}_{\text{cat}}^{-1}) = \frac{F \cdot x \cdot \varphi_i}{W}$$

$F \equiv$ ethanol molar flow fed to the reactor ($\text{mol} \cdot \text{h}^{-1}$)

$W \equiv$ catalyst mass (g)

$\varphi_i \equiv$ Selectivity for the formation of product “i” (moles of C of ethanol converted to component “i”/moles of C of converted ethanol)

Diffuse reflectance infrared Fourier transform (DRIFT) spectroscopy experiments were performed using a Thermo Nicolet Nexus FT-IR equipped with a Smart Collector Accessory and a MCT/A detector. The material (20 mg) was placed inside the catalytic chamber and it was pre-treated at 473 K for 1 h in He flow before the experiment. Spectra were acquired in the $4000\text{-}650 \text{ cm}^{-1}$ wavenumber range, after subtraction of the KBr standard background. The signals were transformed to Kubelka-Munk units to obtain semi-quantitative results. Spectra were recorded at the same temperatures as in the reactor, which enable to compare the evolution of each gas and catalytic surface.

3. Results and discussion

3.1. Characterization of fresh catalysts

Main surface and chemical properties of different catalysts tested in this work are summarized in **Table 1**, whereas HRTEM micrographs with the corresponding histograms and XRD spectra are plotted in **Figure S1** and **S2**, respectively. In general terms, no relevant

changes in the original mixed oxide structure were observed by the presence of metal nanoparticles, being the periclase the main phase in all the cases. Specific surfaces do not suffer significant changes, being the most relevant effect related to a decrease in the acidity and basicity, logical effect due to the metal deposition on their surface. These decreases are more relevant in the case of Ru/Mg-Al, material that presents almost null concentration of strong acid sites and a reduction of more than 90 % of strong basic sites. However, the effects of metal supporting on medium-strength and weak basic and acid sites is very slight. As these sites are the responsible of the aldol condensation (main step catalyzed by acid/basic sites) [29], activity results are directly comparable. Concerning to the crystallite sizes and metal dispersion, similar values were obtained with both metal modified materials, highlighting the high dispersion (more than 75 %) and the consequent small crystallite diameters (around 2 nm). These values are in good agreement with those reported in the literature for similar catalysts prepared by this procedure [30-32].

The low crystallite sizes suggest a strong interaction between metal nanoparticles and support. This hypothesis is congruent with the high reduction temperatures observed by the TPR results (**Figure S3**). Typical reduction temperature for ruthenium particles is proposed at 475 K [33], whereas our catalyst shows the main reduction peak at 580 K. Regarding to the reduction from PdO to Pd⁰, it occurs at very low temperatures, observing a peak around 303 K [34]. Same authors also indicate that palladium has a secondary reduction peak at 353 K. In our case, the reduction peaks appear at higher temperature (321, 414, 579, and 658 K). This reduction temperature shift suggests strong interactions between the metal and the support, such as strong metal-support interaction [35].

3.2. Catalytic study

In order to determine the role of the metal in hydrogenation and dehydrogenation steps, reactions were carried out under inert and reductive conditions. Experimental data obtained with Ru/Mg-Al and Pd/Mg-Al are compared with those obtained with the parent Mg-Al. **Figure 1** shows the 1-butanol productivity, analyzing the evolution as function of the reaction temperature. Maximum temperature, 723 K, as well as the weight hourly space velocity (WHSV = 7.9 h⁻¹) were chosen according to previous results related to the same reaction in absence of any metal phase [16]. In general terms, the most marked effects of the metal presence and hydrogen are observed at the lowest temperatures, reaching similar and almost constant productivities over 650 K, despite the materials or the atmosphere conditions. This fact suggests that at the highest temperatures this reaction is mainly controlled by the chemical properties of the parent mixed oxides with no ~~relevant~~ predominant role of the metal phase. This hypothesis is congruent with the coexistence of two mechanisms: the four-step reaction and the direct ethanol dimerization. The second one is almost negligible at the lowest temperatures whereas its partial relevance cannot be discarded above 623 K. Metals have not any relevant role in the dimerization, being this mechanism only controlled by the acid-basic properties of the catalyst. The coexistence of both mechanisms has been previously reported in the literature [36,37]. Concerning the evolution of the parent material, Mg-Al, same results were obtained despite using inert or reducing conditions. In fact, both series can be hardly distinguished in the plot because most of the points are exactly overlapped. A detailed study of the behavior of this Mg-Al under reducing and inert conditions is reported in our previous work [13]. In general, considering that there is not any metal phase to activate the hydrogen molecule, reducing conditions has no noticeable effect on the behavior of Mg-Al. The 1-butanol production is here conditioned by basic/acid sites that produce the aldol

condensation and hydrogenations by the Meerwein-Ponndorf-Verley (MPV) reduction, needing only Lewis acid and acid-basic pairs [1,38].

The expected enhancement of the 1-butanol productivity derived by the bifunctional material is clearly observed with Ru/Mg-Al. Under inert conditions, at 523 K, the productivity is more than 2.7 times higher than the corresponding one obtained with Mg-Al, suggesting an improvement in the dehydrogenation reaction (first step of the process, determining the amount of acetaldehyde available for the subsequent steps). This enhancement is more relevant under reductive conditions, with values almost 15 times higher for the Ru/Mg-Al at the lowest temperature.

The evolution of ethanol conversion as function of the temperature with the different materials and conditions is shown in **Figure 2**. At the lowest temperatures, conversions obtained with Ru/Mg-Al despite the atmosphere, are very similar (8.2 and 9.2 % at 523 K; 12.3 and 13.0 % at 573 K; 21.0 and 23.4 % at 623 K) suggesting that the presence of hydrogen does not affect the first reaction step. Considering the previously mentioned enhancement in the 1-butanol productivity at these conditions, a relevant role of final hydrogenations is suggested, requiring the ruthenium to activate the molecular hydrogen. However, at the highest temperatures, the differences in the conversion were quite relevant (45.7 and 59.0 % at 723 K, with and without H₂, respectively) but these results do not imply any enhancement in the final 1-butanol production. These results corroborate that direct dimerization is not the main mechanism, even at these temperatures, highlighting the role of intermediate and side-reactions steps, all of them derived from the four-step pathway.

1-Butanol productivity profiles obtained with Pd/Mg-Al were clearly different, with high initial values, followed by a decreasing trend, reaching a minimum at 623 K, after which the

productivity increases again, reaching at the highest temperatures values closed to the obtained with the other materials. This ~~conversion~~ trends are even more evident under reducing conditions, with a more marked productivity minimum. On the contrary, these results correspond to very high palladium conversions, reaching values higher than 65 %. A possible metal sintering as a cause of this behavior was discussed by comparing the metal dispersion of fresh and spent catalysts. After the reaction at the highest temperature, changes in the metal dispersion are lower than 4 %, suggesting an almost negligible role of sintering. Thus, the most likely cause of this unexpected behavior in the double catalytic role of palladium, with probed dehydrogenation activity but also high decarbonylation capacity [22]. Decarbonylation converts acetaldehyde to an equimolar mixture of carbon monoxide and methane. The high relevance of this side reaction is clearly observed when analyzing the high ethanol conversion obtained at medium temperatures (40.4 and 66.3 % at 623 K, under inert and reductive conditions, respectively) and the lack of correspondence with the 1-butanol productivity. The clear negative effect of hydrogen in the case of Pd/Mg-Al suggests a key role of this molecule on the competitive mechanism between condensation and decarbonylation reactions. Methane obtained is directly desorbed and released to the gas phase. However, carbon monoxide is strongly adsorbed on the Pd nanoparticles surface producing its inhibition ~~poisoning~~ [39]. This hypothesis is justified looking at the evolution of CO/CH₄ ratio with the temperature. This magnitude ranges from 0.9 (at 523 K) to 1 (at 723 K). Considering that both compounds are formed with a stoichiometry 1:1, the low concentration of CO detected in the gas phase is congruent with a selective and strong adsorption of this compound. Taking into account the low metal loading, this adsorption can be enough to produce an almost total blockage of metal particles while CO is adsorbed on them.

The CH₄ formation reach a maximum yield of 15.1 % at 623 K, being more relevant under reducing conditions. The recovery of activity at higher temperatures, reaching values similar as those obtained with Mg-Al and Ru/Mg-Al catalysts, corroborates that the inhibition due to CO deposition is reversible at high temperatures, discarding a permanent poisoning and supporting the hypothesis of an inhibition at medium temperatures. The desorption of CO adsorbed on Pd nanoparticles supported on transition oxides at temperatures over 500 K is reported in the literature, indicating that this temperature can be higher as function of the crystallite size and CO initial coverage [40]. As a general conclusion of these results, the role of the noble metals is only ~~relevant~~ decisive at soft and mild conditions, whereas ~~there is not any relevant effect~~ their effect is partially conditioned by the role of acid-basic sites at temperatures over 623 K. This fact is an extra advantage of using these bifunctional materials, reducing the severity of this process. However, in order to have a deeper analysis of this complex mechanism, a systematical analysis in each step, as well as a deep study of side-reactions influence, is required to gain further insights about the role of the metals.

In order to analyze the dehydrogenation ability of these materials, **Figure 3** shows global yield of all the compounds of the main route, formation of acetaldehyde and its further conversion. According to this, "AA + AA derivatives" includes acetaldehyde (AA), ethyl acetate, carbon monoxide, methane, crotonaldehyde, crotyl alcohol, butanal, 1,3-butadiene and butanol, considering their stoichiometric factor. A clear increasing trend was observed in all the cases, reaching the maximum values at the highest temperature tested. A marked improvement was observed for Ru and Pd, even when working under inert conditions, suggesting a significant role of palladium and ruthenium, also in dehydrogenation step. This dehydrogenation capacity is suggested considering only the relative comparison among materials under inert conditions. The improvements when working under reducing conditions

are directly related to the influence of subsequent steps (hydrogenations) in the global reaction and cannot be directly assumed as dehydrogenation abilities. Results obtained with palladium at temperatures under 650 K are strongly conditioned by the decarbonylation step, side reaction that requires the dehydrogenation of ethanol into acetaldehyde. Accordingly, the good behavior of this material in this partial analysis is not directly related to a higher 1-butanol productivity.

In order to complete the study of the first step, the relative weight of dehydration side-reactions is analyzed in **Figure 4**. In this plot, the global selectivity of acetaldehyde and all its derivatives is related to the global selectivity of all the products identified in **Scheme 1**. According to this, the decreasing trends observed with both, Mg-Al and Ru/Mg-Al, are directly related to an increasing weight of dehydration steps, consuming ethanol for obtaining ethylene and diethyl ether. These results are in good agreement with the sharper increase of the dehydration rates with the temperature reported in the literature [14]. This trend is much more marked with Mg-Al than with Ru/Mg-Al, being directly related to the different acidity and basicity of both materials. In fact, there are two main dehydration mechanisms, involving different type of sites: Lewis acid-Bronsted base pair for the E_2 and strong basic sites and weak Lewis acids for the E_{1CB} mechanism [14]. Both metals block most of the Lewis acid sites, whereas the strong basic ones only disappear in the Ru/Mg-Al. Considering the high selectivity of Ru/Mg-Al for the main route, these sites are proposed as the most active ones to catalyze dehydration reactions. In good agreement with this premise, ethanol dehydrations when Mg-Al mixed oxide is present mainly occur following an E_{1CB} mechanism, being catalyzed by strong basic sites. The almost total blockage of these sites by ruthenium nanoparticles justify the highest selectivity to acetaldehyde and derivatives observed with this material. With the Ru/Mg-Al, ethylene is the main dehydration product (from 2.3 to 19.4 %, at 523 and 723 K,

respectively), whereas less than 4 % of diethyl ether was observed. The role of hydrogen in this dehydration steps is almost negligible for the Ru/Mg-Al because the adsorption occurs on the metal sites, no disturbing processes catalyzed by acid/basic sites. The different behavior observed with Mg-Al and Pd/Mg-Al is explained by the competitive adsorption of hydrogen molecules and the ethoxide (intermediate obtained during the ethanol dehydrogenation) on acid/basic sites [13]. The interaction between Mg-Al and hydrogen molecule (even in absence of metal sites) has been previously observed in the literature, concluding that this effect is less relevant at high temperatures, as the importance of OH sites decreases [41,42]. Regarding to Pd/Mg-Al, under 650 K, most of the metal sites are ~~poisoned~~ covered by the CO, being the acid/basic sites the only available ones (similarly to the parent oxide). According to this hypothesis, for these materials, side reactions are enhanced under reducing conditions, with ethylene selectivities up to 34.5 % and diethyl ether selectivities higher than 10 % (Mg-Al at 723 K). In good agreement with this competitive behavior, conversions obtained with these materials do not suffer the clear enhancement obtained with the Ru/Mg-Al when hydrogen is introduced in the medium (from 53.8 to 43.1 % at 723 K with Mg-Al; from 45.7 to 59 % with Ru/Mg-Al; and from 47.7 to 49.0 % with Pd/Mg-Al).

Figure 5 illustrates the relative weight of aldol condensation, analyzing the global selectivity of aldolization products (crotonaldehyde, crotyl alcohol, butanal, 1,3-butadiene and 1-butanol) in comparison to the global selectivity to products obtained from acetaldehyde (identified before as “AA derivatives”). In the cases of Mg-Al and Ru/Mg-Al, a very high selectivity to main reaction is observed, obtaining in all the cases condensation ratios higher than 90 %, for both materials and not depending on the hydrogen presence. The parallel behavior shown by both materials, independently of the type of atmosphere, is in good agreement with the general mechanism of aldol condensation, where medium-strength basic

sites are the main responsible of the catalytic activity, prevailing these types of sites over the any catalytic effect of the metal nanoparticles [13,29]. Basicity analysis by temperature programmed desorption studies demonstrate the almost null effect of supporting ruthenium on Mg-Al on the medium-strength basicity, keeping constant more than 85 % of the initial concentration of these type of sites. With these materials, ethyl acetate was the only side product observed, being the responsible of the soft decrease observed at the lowest temperatures. This result is congruent with the more direct esterification mechanism, in contrast to the aldolization, which requires the enolate intermediate specie [43]. As it was previously reported for cobalt and nickel metals, the presence of metals and hydrogen inhibits to some degree the formation of the enolate intermediate from acetaldehyde (β C-H scission hindered by hydrogen adatoms), enhancing the selectivity to the esterification pathway [13]. According to this premise, despite being very selective to aldolization at any temperature, the selectivity is a bit lower at soft conditions because of the presence of ethyl acetate below 600 K. ~~On the other hand, decarbonylation products were not observed, neither with Mg-Al nor with Ru/Mg-Al.~~ On the other hand, a low but quantifiable amount of CO and CH₄ is observed with Ru/Mg-Al under inert conditions, justifying the lower selectivity observed at soft temperatures. Decarbonylation products are formed at low extent, being this extent almost constant at all the temperatures. Therefore, the relative weight of this reaction in the global selectivity decreases as temperature increases. Thus, in general terms, the second main conclusion of these results is the negligible role of hydrogen in the aldol condensation step, obtaining same relative weight despite the presence or absence of hydrogen.

Pd/Mg-Al requires a specific analysis. With this material, the role of decarbonylation strongly affects these results, justifying the inverted volcano profile obtained. As it was previously suggested, the relative weight of this side reaction increased with the temperature

and reached its maximum at 623 K, temperature at which the minimum relative weight of the aldol mechanism was observed (it must be reminded that carbon monoxide and methane are involved in the “AA derivatives” term). At these conditions, individual selectivities close to 12 and 13 % of CH₄, under inert and reductive conditions, respectively, were detected. These values are more than one hundred times higher than the maximum ones obtained with Ru/Mg-Al. If the role of carbon monoxide and methane in this analysis is discarded, profiles obtained with Ru and Pd are overlapped, with selectivities for aldol condensation higher than 93 %, corroborating ethyl acetate is only quantified at temperatures under 600 K and in low amounts. In good agreement, if aldolization capacity is analyzed in terms of global production, an enhancement higher than 20 % respect to the bulk material is obtained (1342 and 1678 mol·g⁻¹·ks⁻¹, for Mg-Al and Pd/Mg-Al at 723 K, respectively).

The effect of the metals and their ~~CO-poisoning~~ CO-inhibition is even more evident when analyzing the relative weight of hydrogenation (conditioned by the activity of nanoparticles) and dehydration (conditioned by strong acid sites) steps. This comparison is illustrated in **Figure 6**, as the ratio between 1,3-butadiene and 1-butanol. As expected, parallel evolution was observed in the case of Mg-Al, with a high increase of the dehydration selectivity at the highest temperatures. The slight difference observed between inert and reducing conditions (mainly at soft temperatures) is justified by an interaction between hydrogen and support, by a non-dissociative adsorption of this molecule on the strong acid sites (OH, sites responsible of dehydration) [14,42]. According to this mechanism, hydrogenation steps are slightly promoted even in absence of metal phases. This effect disappeared at high temperature because of the exothermic character of adsorption process, recovering the dehydration capacity. Ru/Mg-Al profiles follow the same trend, with almost negligible role of reducing conditions. These values are justified by the dehydrogenating character of ruthenium [44,45],

being also congruent with the results previously explained in the analysis of dehydrogenation step. As a consequence of this dehydrogenation capacity, not only the last steps of the main route were hindered, enhancing the crotonaldehyde selectivity, but also part of 1-butanol obtained suffers dehydrogenation in its alcohol functionality, obtaining butanal. In good agreement with this statement, the production ratio between crotonaldehyde and butanal to 1-butanol reaches values 1.7 times higher with Ru/Mg-Al (0.81) than with the parent Mg-Al (0.47), under inert conditions at 723 K (temperature at which the dehydrogenation is more favored). Same ratio decreases to values close to 1.4 when results under reducing conditions are compared, confirming the enhancement of hydrogenation mechanism because of the presence of hydrogen. These results are higher than the corresponding ones obtained when transition metals were used (ratios of 0.61 and 0.48 with Co/Mg-Al and Ni/Mg-Al, respectively) [13], demonstrating a significant dehydrogenation activity of ruthenium. In addition to this reason, a partial capacity to activate the hydrogen molecule, even under inert conditions, cannot be discarded, considering the high hydrogenation activity of Ru nanoparticles.

As in the previous steps, the profile obtained with palladium catalysts suggests different predominant reactions as temperature changes. First part of the graph (temperatures up to 623 K) indicates an increasing trend with the temperature. This result is congruent with the previously mentioned ~~poisoning~~ inhibition of palladium nanoparticles by the presence of carbon monoxide adsorbed on their surface. This adsorption occurs mainly on the nanoparticles, hindering the last steps of the main mechanism (hydrogenations that require the metal) because metal sites are ~~poisoned~~ blocked by the presence of CO. However, nanoparticles do not have any relevant role in dehydration step, being possible the transformation of the crotyl alcohol into 1,3-butadiene. Based on this hypothesis, this effect is

more evident under inert conditions because the presence of molecular hydrogen in excess, under reducing conditions, makes possible the hydrogenations on acid/basic sites promoted by the MPV reduction, enhancing the production of 1-butanol, but in a significant lower proportion as expected. At temperatures over 623 K, the behavior of Pd/Mg-Al is quite different, being congruent with the recovery of metal activity. Under inert conditions, the expected behavior is observed, with an increase of the relative weight of dehydrations (similar trend as with Mg-Al and Ru/Mg-Al). However, under reducing conditions, the strong hydrogenation activity of palladium nanoparticles is clearly observed, discarding a permanent poisoning and supporting the CO desorption at these conditions, obtaining a dehydration/hydrogenation ratio much lower than in the other cases. According to this analysis, experimental results confirm the high hydrogenation activity of palladium nanoparticles, as it was previously observed in the literature [46].

All the hypothesis suggested in this study were checked by analyzing not only the composition of the gas phase, but also evaluating the different species adsorbed on the catalytic surface, in order to identify changes in the adsorption modes and intensities. This parallel study was carried out by DRIFT spectroscopy, reproducing the same environmental conditions as in the fixed bed reactor. To identify the most relevant conclusions, **Figure 7a** shows the different spectra obtained under inert atmosphere, whereas the results obtained at same conditions but under reducing atmosphere are plotted in **Figure 7b**. In general, three main interesting regions are observed. The first one is identified as the stretching mode of C-O (cm^{-1}) [16], being related to the adsorption of alkoxide species. The second one, at 1580 cm^{-1} , corresponds to the stretching vibration mode of C=C bonds (unsaturated alcohols and aldehydes), such as the crotonaldehyde and crotyl alcohol [16]. The third band, at 1740 cm^{-1} , is associated with the stretching vibration mode of C=O of aldehydes [16]. There are other

two bands clearly observed, at 950 and 1440 cm^{-1} , approximately. These bands correspond to common vibration modes of C-H₃ (rocking and deforming one, respectively) [16], so they are not useful to identify any relevant molecule. The area of these bands can only be related to the amount of heavy compounds adsorbed on the catalytic surface. For all the bands, highest intensities are in good agreement with the highest concentration of acid sites (more than six times higher with Mg-Al than with the metal-modified materials), because of the higher ability to stabilize compounds [47]. As to the Mg-Al, the typical decrease in the intensities of the peaks is clearly observed, in good agreement with the exothermic character of adsorption. However, signals at 723 K are still more intense than those obtained with ruthenium and palladium metal-modified materials, even at 523 K. This comparison suggests that the adsorption of aldehydes and alcohols is stronger with this material. As a direct consequence of this adsorption, the oligomerization can be promoted, obtaining heavier unsaturated compounds. These compounds might be permanently adsorbed on Mg-Al surface, being the reason of the lowest carbon balance obtained with this material (63.2, 84.7, 75.0 % for Mg-Al, Ru/Mg-Al and Pd/Mg-Al, at 723 K, respectively). The higher intensity observed under inert conditions is directly related to the positive effect of hydrogen in the stability of these materials, decreasing the amount of unsaturated compounds and preventing their adsorption blocking the active sites. Concerning the ruthenium, same peaks as for the Mg-Al were detected, being the adsorption intensities significantly lower and observing a continuous decrease at increasing temperatures. On the contrary, spectra of palladium at 523 and 623 K are overlapped, observing only a slight evolution at 723 K. This result is congruent with a different behavior of this material at temperature under and over 623 K.

The hypothesis of metal poisoning by permanent chemisorption inhibition by adsorption of CO molecules is corroborated by analyzing the signals in the range 1900 – 2300 cm^{-1} .

According to the literature [47], a ~~high~~ quite relevant CO coverage (from 60 to 70 %) on a well-ordered Pd (111) is related to two intense bands observed at 1966 and 2092 cm^{-1} . As it is observed in **Figure 8**, these signals are clearly identified in the case of Pd/Mg-Al, at 1990 and 2020 cm^{-1} wavenumbers, respectively. The observed shifts are justified by the interaction between small nanoparticles and the mixed oxide surface). In the case of Pd/Mg-Al, there is a clear increasing trend in these intensities when temperature rises from 523 to 623 K, whereas these signals slightly decrease at more severe conditions. This evolution is in agreement with results observed in the gas phase analyses. In good agreement with the high concentration of CO observed in the gas phase, main signals related to this compound are in the range 2120 – 2200 cm^{-1} wavenumbers, which correspond to the CO in gas phase signal. On the contrary, as it is observed in **Figure 9**, Ru exhibits lower decarbonylation activity in the gas phase, but its interaction with this metal is stronger than in the case of Pd (binding energies of -162 and -104 kJ/mol for Ru and Pd, respectively [22]). In good agreement with these premises, almost null signal in the range of free CO is observed, whereas there is a clear band around 2020 - 2035 cm^{-1} , specific band corresponding to a low coverage of Ru particles by CO chemisorption, as it is identified in the literature [49]. DRIFT spectra allow corroborating the deactivation of Pd particles by CO adsorption, confirming the different activity of Pd and Ru, being the first one clearly conditioned by decarbonylation reactions. According to activity results, the partial coverage of Ru by CO is not relevant in the global activity of this material, concluding that decarbonylation kinetics prevails over chemisorption capacity.

In **Figure 7b**, parallel spectra are analyzed, but under reducing conditions. Despite Kubelka-Munk is only a semiquantitative methodology, same scale was used for both cases, in order to compare the intensities of same bands under different conditions. As it is clear observed, lower effects are noticed with Mg-Al, with spectra where same bands are clearly

identified. According to the high relevance of hydrogenation steps, under reducing conditions the band at 1740 cm^{-1} disappears (corresponding to crotonaldehyde observed under inert conditions). Special attention must be devoted to the palladium modified material spectrum. With this catalyst, only slight adsorptions were observed, except for the band at 950 and 730 cm^{-1} . The last one has been previously related to heavy compounds, characteristically of the CH_2 rocking vibration mode of molecules with more than four of these groups [50]. Thus, it is assumed to be directly related to the heavier products observed when the reaction is not limited to 1-butanol. With this material, the CO deposition blocks the palladium nanoparticle, only affecting the hydrogenation activity but keeping intact the activity for the subsequent oligomerization reactions from crotonaldehyde. This band is, consequently, in good agreement with the lower carbon balance obtained with this material.

4. Conclusions

The addition of a reduced metal to basic mixed oxides improves their performance for 1-butanol formation at low temperatures, especially in the presence of hydrogen reaching productivities up to 15 times higher than those corresponding to the Mg-Al. In absence of hydrogen, a relevant improvement in the dehydrogenation step was observed, being more evident with the Ru-doped material. With this metal, the acetaldehyde yields increases 75 % on the value obtained with the non-modified Mg-Al. This material does not exhibit a highlighting role in hydrogenations. Considering the high improvement in the production of 1-butanol, the ethanol-to-acetaldehyde dehydrogenation step is identified as the rate-determining one.

The palladium behavior is strongly conditioned by the decarbonylation side-product, promoted when temperature is lower than 650 K. As a consequence, at soft temperatures the improvement of the 1-butanol productivity is also consistent with a high dehydrogenation activity, whereas the improvement at higher temperatures is due to the high hydrogenation ability.

According to DRIFT spectroscopy, ethoxides are identified as the main species adsorbed on the mixed oxide catalyst, being this adsorption much more relevant with the parent material than with the metal modified ones, mainly under inert conditions. These results are in good agreement with the hypothesis of an improvement in the stability by adding metal nanoparticles because of the lower saturation of catalytic surface by unsaturated compounds.

Acknowledgments

Founding from the MINECO (Ministry of Economy and Competitiveness) of the Government of Spain (Contracts: CTQ2014-52956-C3-1-R and CTQ2017-89443-C3-2-R). Jorge Quesada thanks the Government of the Principality of Asturias for his PhD fellowship of the Severo Ochoa Program (PA-14-PF-BP14-105).

References

- [1] T. Moteki, D. W. Flaherty, *ACS Catal.* 6 (2016) 4170-4183.
- [2] L. Faba, E. Díaz, S. Ordóñez, *Renew. Sustain. Energy Reviews* 51 (2015) 273-287.
- [3] M. J. Climent, A. Corma, V. Fornés, R. Guil-López, S. Iborra, *Adv. Synth. Catal.* 344 (2002) 1090-1096.

- [4] J. I. Di Cosimo, V. K. Díez, C. R. Apesteguía, *Appl. Catal. A* 137 (1996) 149-166.
- [5] G. Zhang, H. Hattori, K. Tanabe, *Appl. Catal.* 36 (1988) 189-197.
- [6] G. R. M. Dowson, M. F. Haddow, J. Lee, R. L. Wingad, D. F. Wass, *Angew. Chem. Int. Ed.* 52 (2013) 9005-9008.
- [7] T. Riittonen, K. Eränen, P. Mäki-Arvela, A. Shchukarev, A. R. Rautio, K. Kordas, N. Kumar, T. Salmi, J. P. Mikkola, *Renew. Energy* 74 (2015) 369-378.
- [8] I. C. Freitas, S. Damyanova, D. C. Oliveira, C. M. P. Marques, J. M. C. Bueno, *J. Mol. Catal. A* 381 (2014) 26-37.
- [9] J. H. Earley, R. A. Bourne, M. J. Watson, M. Poliakoff, *Green Chem.* 17 (2015) 3018-3025.
- [10] X. Wu, G. Fang, Z. Liang, W. Leng, K. Xu, D. Jiang, J. Ni, X. Li, *Catal. Commun.* 100 (2017) 15-18.
- [11] J. Pang, M. Zheng, L. He, L. Li, X. Pan, A. Wang, X. Wang, T. Zhang, *J. Catal.* 344 (2016) 184-193.
- [12] T. Riittonen, E. Toukoniitty, D. K. Madnani, A. R. Leino, K. Kordas, M. Szabo, A. Sapi, K. Arve, J. Wärnå, J. P. Mikkola, *Catalysts* 2 (2012) 68-84.
- [13] J. Quesada, L. Faba, E. Díaz, S. Ordóñez, *Appl. Catal. A* 559 (2018) 167-174.
- [14] J. I. Di Cosimo, C. R. Apesteguía, M. J. L. Ginés, E. Iglesia, *J. Catal.* 190 (2000) 261-275.
- [15] S. Ordóñez, E. Díaz, M. León, L. Faba, *Catal. Today* 167 (2011) 71-76.
- [16] J. Quesada, L. Faba, E. Díaz, S. Ordóñez, *Appl. Catal. A* 542 (2017) 271-281.
- [17] M. Farrag, *Micropor. Mesopor. Mat.* 257 (2018) 110-117.
- [18] T. J. Schwartz, B. H. Shanks, J. A. Dumesic, *Curr. Opin. Biotechnol.* 38 (2016) 54-62.
- [19] M. Kolodziej, E. Lalik, J. C. Colmenares, P. Lisowski, J. Gurgul, D. Duraczyńska, A. Drelinkiewicz, *Mater. Chem. Phys.* 204 (2018) 361-372.

- [20] M. A. Vannice, B. Sen, *J. Catal.* 115 (1989) 65-78.
- [21] B. Bachiller-Baeza, I. Rodríguez-Ramos, A. Guerrero-Ruiz, *Appl. Catal. A* 205 (2001) 227-237.
- [22] E. I. Gürbüz, D. D. Hibbitts, E. Iglesia, *J. Am. Chem. Soc.* 137 (2015) 11984-11995.
- [23] L. Yin, J. Liebscher, *Chem. Rev.* 107 (2007) 133-173.
- [24] D. Wang, D. Astruc, *Chem. Rev.* 115 (2015) 6621-6686.
- [25] D. Morton, D. J. Cole-Hamilton, I. D. Utuk, M. Paneque-Sosa, M. López-Póveda, *J. Chem. Soc., Dalton Trans.* 0 (1989) 489-495.
- [26] M. Nielsen, A. Kammer, D. Cozzula, H. Junge, S. Gladiali, M. Beller, *Angew. Chem.* 123 (2011) 9767-9771.
- [27] E. Kossoy, Y. Diskin-Posner, G. Leituss, D. Milstein, *Adv. Synth. Catal.* 354 (2012) 497-504.
- [28] M. León, E. Díaz, S. Ordóñez, *Catal. Today* 164 (2011) 436-442.
- [29] L. Faba, E. Díaz, S. Ordóñez, *Appl. Catal. B* 142-143 (2013) 387-395.
- [30] I. Obregón, I. Gandarias, A. Ocio, I. García-García, N. Álvarez de Eulate, P. L. Arias, *Appl. Catal. B* 210 (2017) 328-341.
- [31] A. Guerrero, M. Reading, Y. Grillet, J. Rouquerol, J. P. Boitiaux, J. Cosyns, *J. Phys. D – Atoms Molec. Clusters* 12 (1989) 583-586.
- [32] K. L. Luska, P. Miglowski, S. E. Sayed, W. Leitner, *ACS Sustain. Chem. Eng.* 4 (2016) 6186-6192.
- [33] P. G. J. Koopman, A. P. G. Kleboom, H. van Bekkum, *J. Catal.* 69 (1981) 172-179.
- [34] C. B. Wang, H. K. Lin, C. M. Ho, *J. Mol. Catal. A* 180 (2002) 285-291.
- [35] G. C. Bond, *Metal-Catalysed Reactions of Hydrocarbons*, Eds.: M. V. Twigg and M. S. Spencer, Springer, New York, 2005, pp. 133, 137.
- [36] M.J.L. Gines, E. Iglesia, *J. Catal.* 176 (1998) 155-172.

- [37] X. Wu, G. Fang, Y. Tong, D. Jiang, Z. Liang, W. Leng, L. Liu, P. Tu, H. Wang, J. Ni, X. Li, *ChemSusChem* 11, 2018, 71-85.
- [38] J. J. Ramos, V. K. Díez, C. A. Ferretti, P. A. Torresi, C. R. Apesteguía, J. I. Di Cosimo, *Catal. Today* 172 (2011) 41-47.
- [39] T. Bligaard, J. K. Nørskov, S. Dahl, J. Matthiesen, C. H. Christensen, J. Sehested, *J. Catal.* 224 (2004) 206-217.
- [40] M. Bäumer, J. Libuda, A. Sandell, H.J. Freund, G. Graw, T. Bertrams, H. Neddermeyer, B. Bunsenges, *Phys. Chem.* 99 (1995) 1381-1386.
- [41] M. Boudart, A. Delvouille, E.G. Derounane, V. Indovina, A.B. Walters, *J. Am. Chem. Soc.* 94 (1972) 6622-6630.
- [42] D. D. Eley, M. A. Zammit, *J. Catal.* 21 (1971) 377-383.
- [43] M. E. Sad, N. Neurock, E. Iglesia, *J. Am. Chem. Soc.* 133 (2011) 20384-20398.
- [44] M. Nielsen, E. Alberico, W. Baumann, H. J. Drexler, H. Junge, S. Gladiali, M. Beller, *Nature* 495 (2013) 85-89.
- [45] R.E. Rodríguez-Lugo, M. Trincado, M. Vogt, F. Tewes, G. Santiso-Quinones, H. Grützmacher, *Nat. Chem.* 5 (2013) 342-347.
- [46] H.U. Blaser, A. Schnyder, H. Steiner, F. Rössler, P. Baumeister, 2nd ed., G. Ertl, H. Knözinger, F. Schüth, J. Weitkamp (Eds.), *Handbook of Heterogeneous Catalysis*, vol. 7, Wiley VCH, Weinheim, 2008, p. 3286.
- [47] C. L. Kibby, W. K. Hall, *J. Catal.* 29 (1973) 144-159.
- [48] K. Wolter, O. Seiferth, H. Kuhlenbeck, M. Bäumer, H. J. Freund, *Surf. Sci.* 399 (1998) 190-198.
- [49] J. Schwank, G. Parravano, H.L. Gruber, *J. Catal.* 61 (1980) 19-28.

[50] B. C. Smith, *Infrared Spectral Interpretation: A Systematic Approach*, CRC Press LLC, Florida, 1999, p. 36.

SCHEME CAPTION

Scheme 1. Proposed reaction mechanism in the ethanol condensation.

FIGURE CAPTION

Figure 1. 1-butanol productivity as function of the reaction temperature when ethanol gas-phase condensation is carried out using Mg-Al (circles), Pd/Mg-Al (triangles) or Ru/Mg-Al (diamonds). Void symbols correspond to inert atmosphere, whereas black ones correspond to reducing conditions

Figure 2. Ethanol conversion evolution with the temperature under inert (void symbols) and reducing conditions (black ones). Results correspond to Mg-Al (circles); Ru/Mg-Al (diamonds); Pd/Mg-Al (triangles)

Figure 3. Dehydrogenation activity as function of the reaction temperature studied in terms of global yield (η). "AA" corresponds to acetaldehyde, whereas "AA derivatives" involves the global selectivity to crotonaldehyde, butanal, crotyl alcohol, 1,3-butadiene, 1-butanol, ethyl acetate, carbon monoxide and methane. (*See figure 1 for codes*)

Figure 4. Relative selectivity to dehydrogenation route. "AA" corresponds to acetaldehyde, whereas "AA derivatives" involves the global selectivity to crotonaldehyde, butanal, crotyl alcohol, 1,3-butadiene, 1-butanol, ethyl acetate, carbon monoxide and methane. (*See figure 1 for codes*)

Figure 5. Condensation activity as function of the reaction temperature. "aldol." corresponds to the global selectivity to crotonaldehyde, crotyl alcohol, butanal, 1,3-butadiene and 1-butanol. (*See figure 1 for codes*)

Figure 6. Relative selectivity of dehydration vs. hydrogenation activity, as function of the ratio between 1,3-butadiene and 1-butanol. (*See figure 1 for codes*)

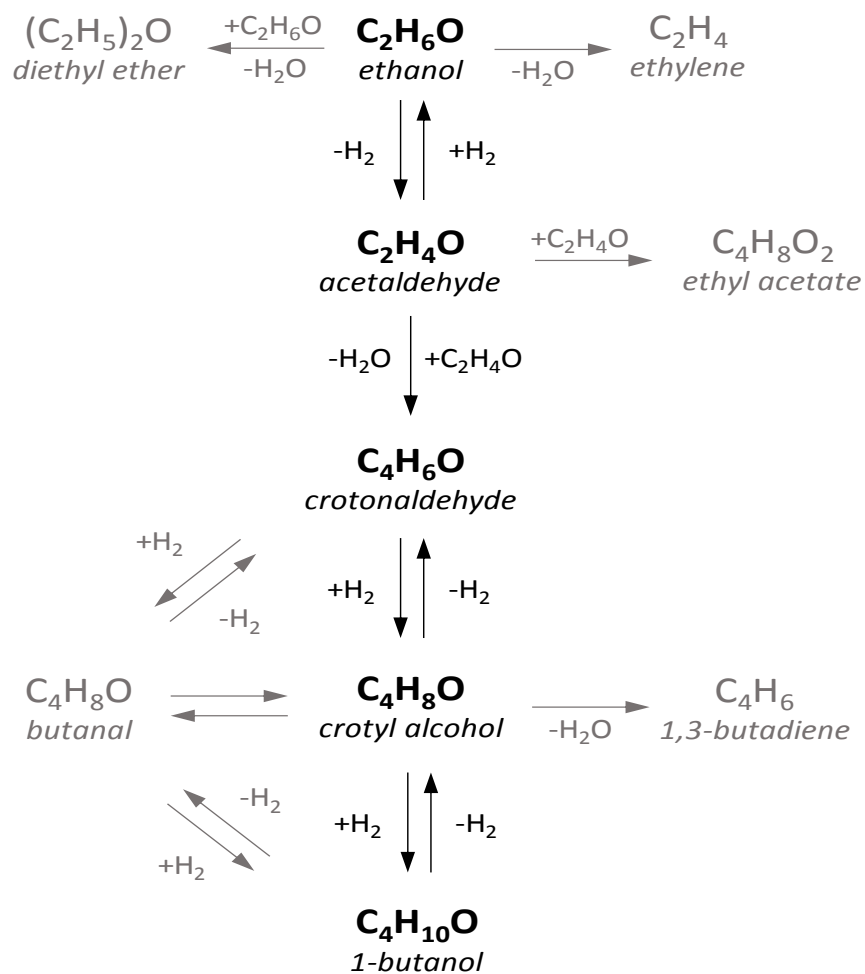
Figure 7. Comparison of DRIFT spectra obtained under (a) inert and (b) reducing conditions with the different materials at the most significant temperatures: 523 K (continuous line); 623 K (broken line); 723 K (dotted line).

Figure 8. Detailed DRIFT spectra in the ranges of CO signals on Pd/Mg-Al surface as function of the temperature. Spectra focused on the area of (a) adsorbed CO; and (b) gas-phase free CO.

Figure 9. Detailed DRIFT spectra in the ranges of CO signals on Ru/Mg-Al surface as function of the temperature. Spectra focused on the area of (a) adsorbed CO; and (b) gas-phase free CO.

TABLE CAPTION

Table 1. Main results of the fresh catalysts characterization: morphological properties, density and distribution of the acid and basic sites, reduction temperature, and HRTEM results.



Scheme 1. Proposed reaction mechanism in the ethanol condensation.

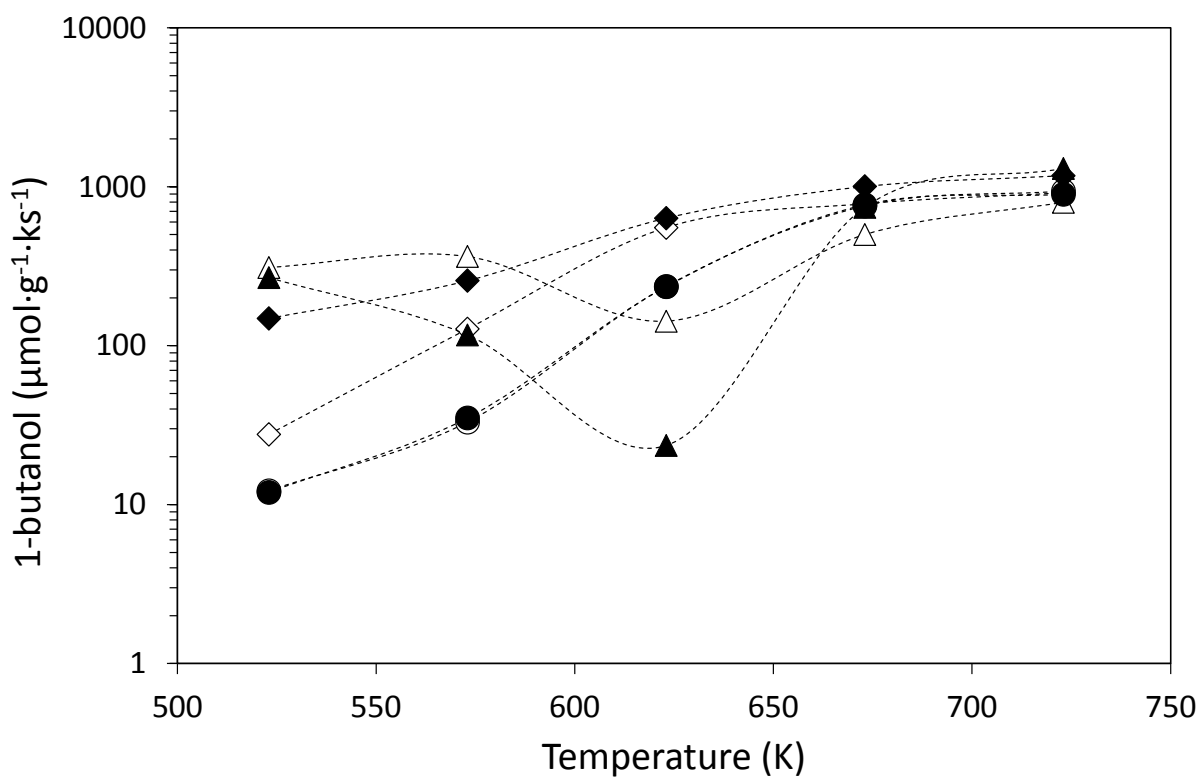


Figure 1. 1-butanol productivity as function of the reaction temperature when ethanol gas-phase condensation is carried out using Mg-Al (circles), Pd/Mg-Al (triangles) or Ru/Mg-Al (diamonds). Void symbols correspond to inert atmosphere, whereas black ones correspond to reducing conditions

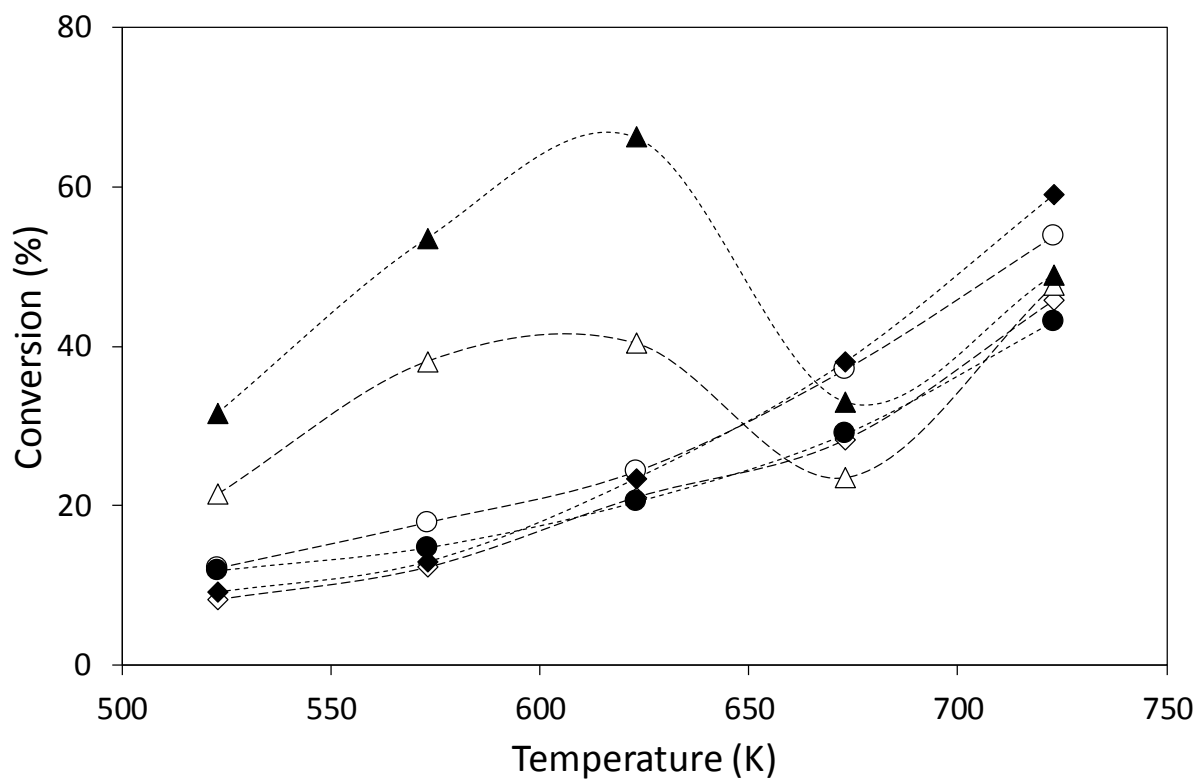


Figure 2. Ethanol conversion evolution with the temperature under inert (void symbols) and reducing conditions (black ones). Results correspond to Mg-Al (circles); Ru/Mg-Al (diamonds); Pd/Mg-Al (triangles)

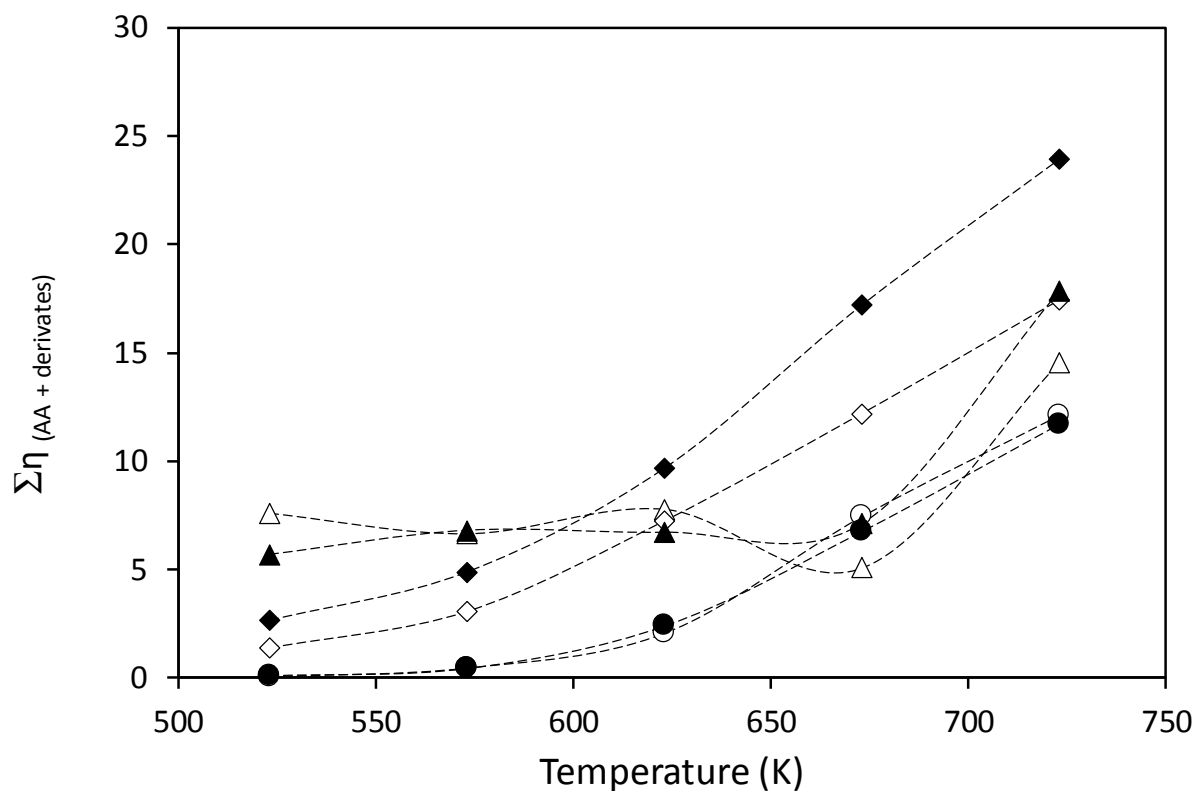


Figure 3. Dehydrogenation activity as function of the reaction temperature studied in terms of global yield (τ). “AA” corresponds to acetaldehyde, whereas “AA derivatives” involves the global selectivity to crotonaldehyde, butanal, crotyl alcohol, 1,3-butadiene, 1-butanol, ethyl acetate, carbon monoxide and methane. (See figure 1 for codes)

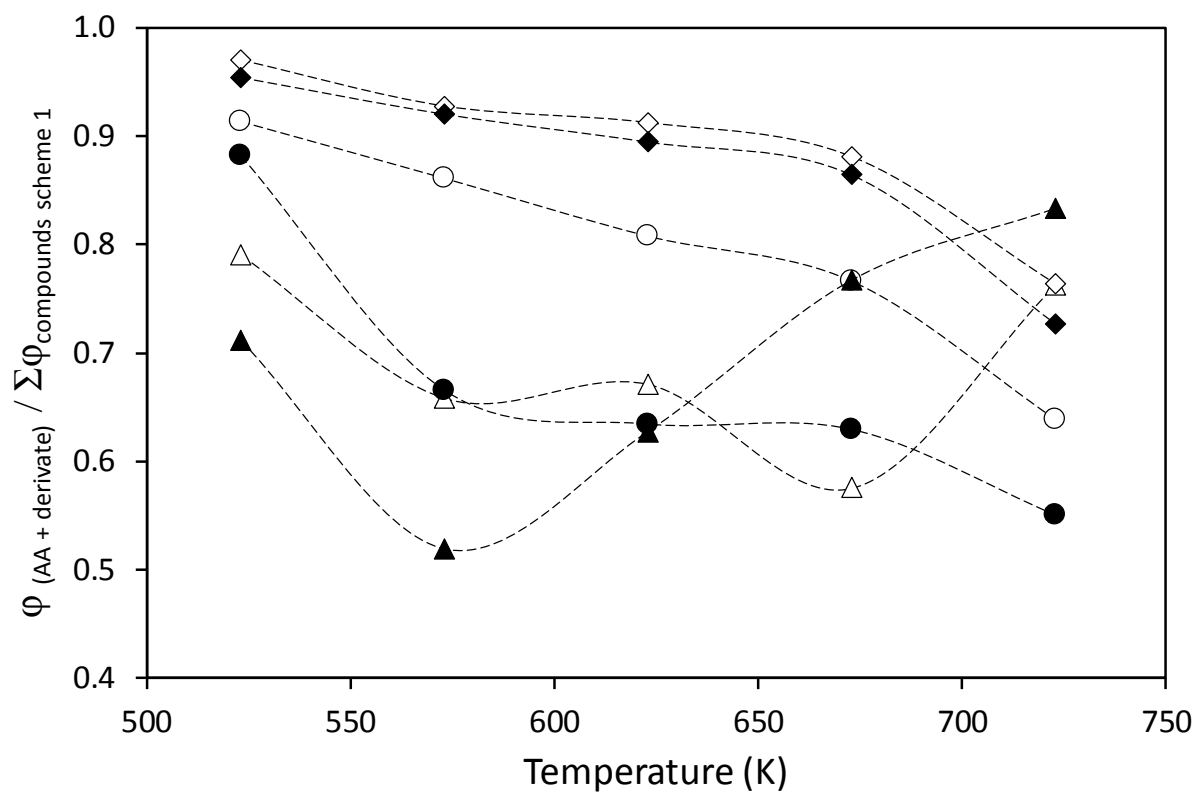


Figure 4. Relative selectivity to dehydrogenation route. “AA” corresponds to acetaldehyde, whereas “AA derivatives” involves the global selectivity to crotonaldehyde, butanal, crotyl alcohol, 1,3-butadiene, 1-butanol, ethyl acetate, carbon monoxide and methane. (See figure 1 for codes)

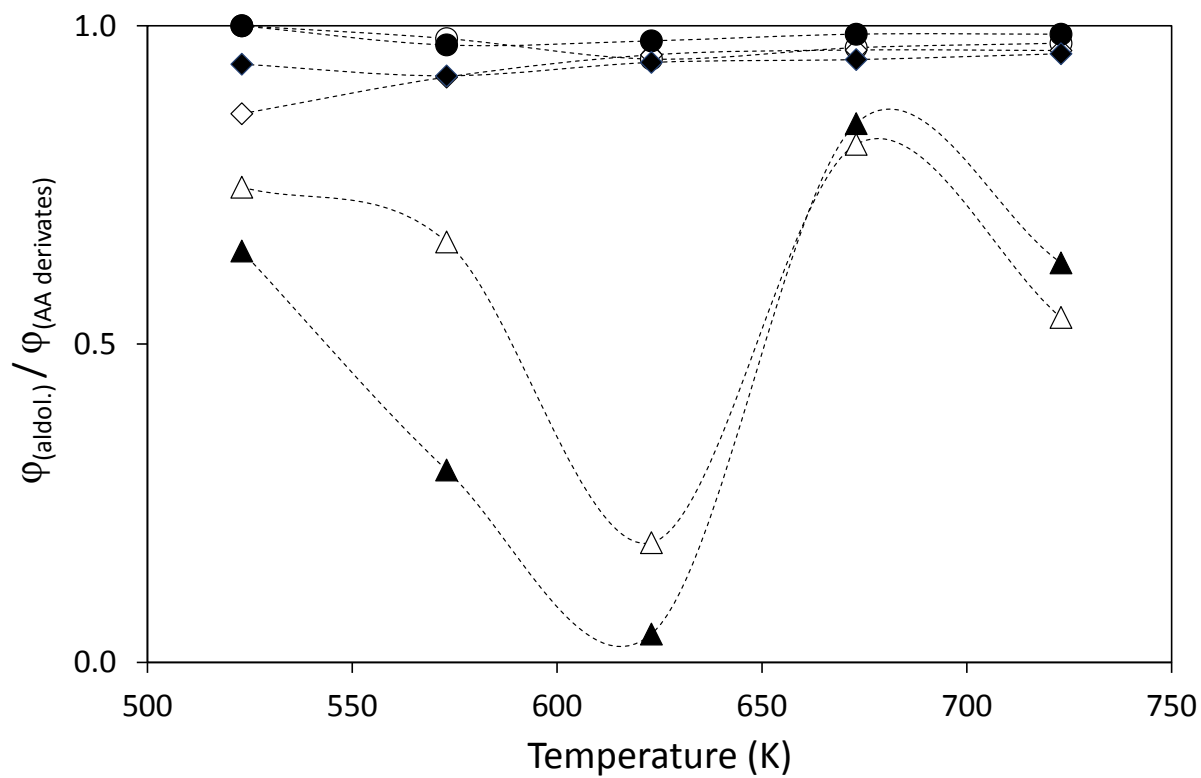


Figure 5. Condensation activity as function of the reaction temperature. “aldol.” corresponds to the global selectivity to crotonaldehyde, crotyl alcohol, butanal, 1,3-butadiene and 1-butanol. (See figure 1 for codes)

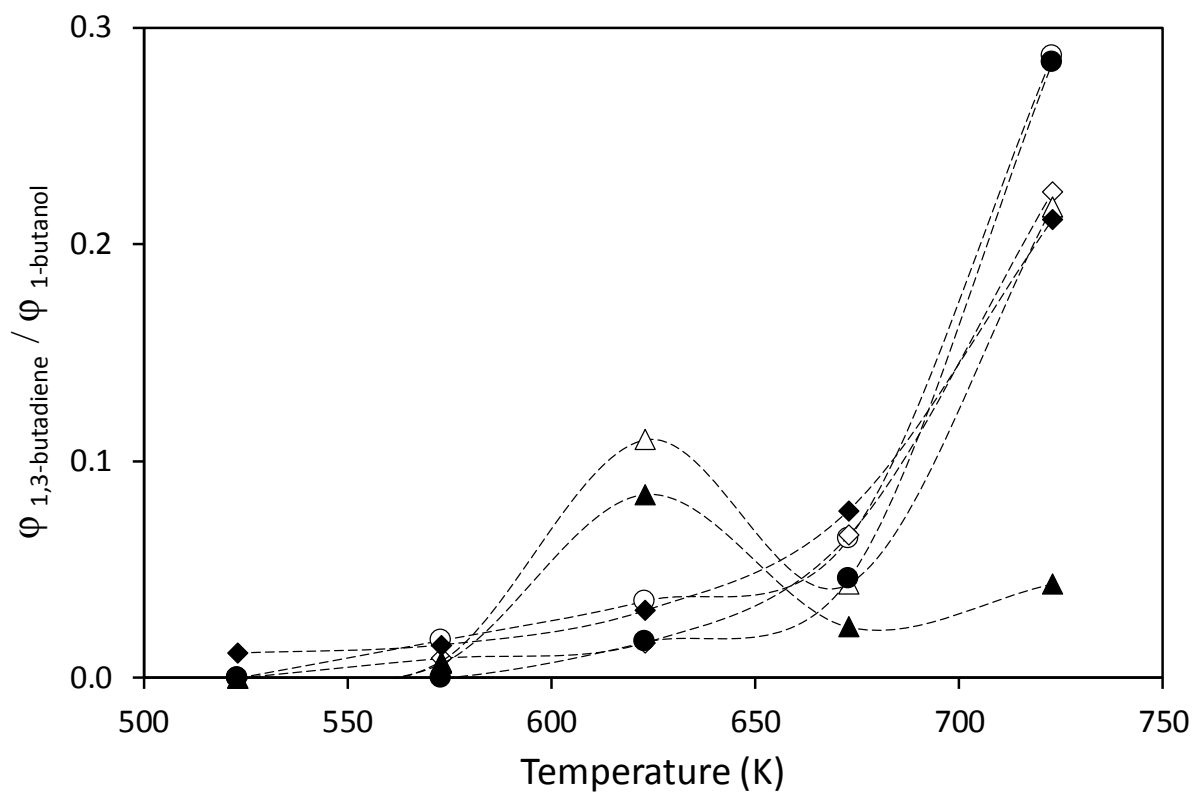


Figure 6. Relative selectivity of dehydration vs. hydrogenation activity, as function of the ratio between 1,3-butadiene and 1-butanol. (See figure 1 for codes)

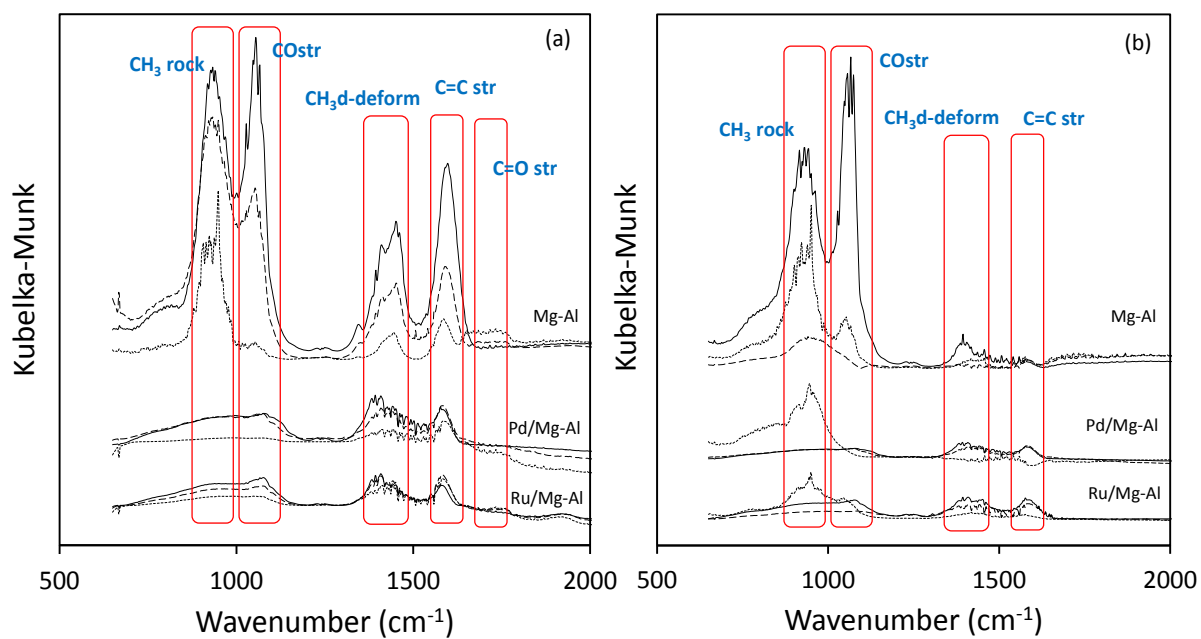


Figure 7. Comparison of DRIFT spectra obtained under (a) inert and (b) reducing conditions with the different materials at the most significant temperatures: 523 K (continuous line); 623 K (broken line); 723 K (dotted line).

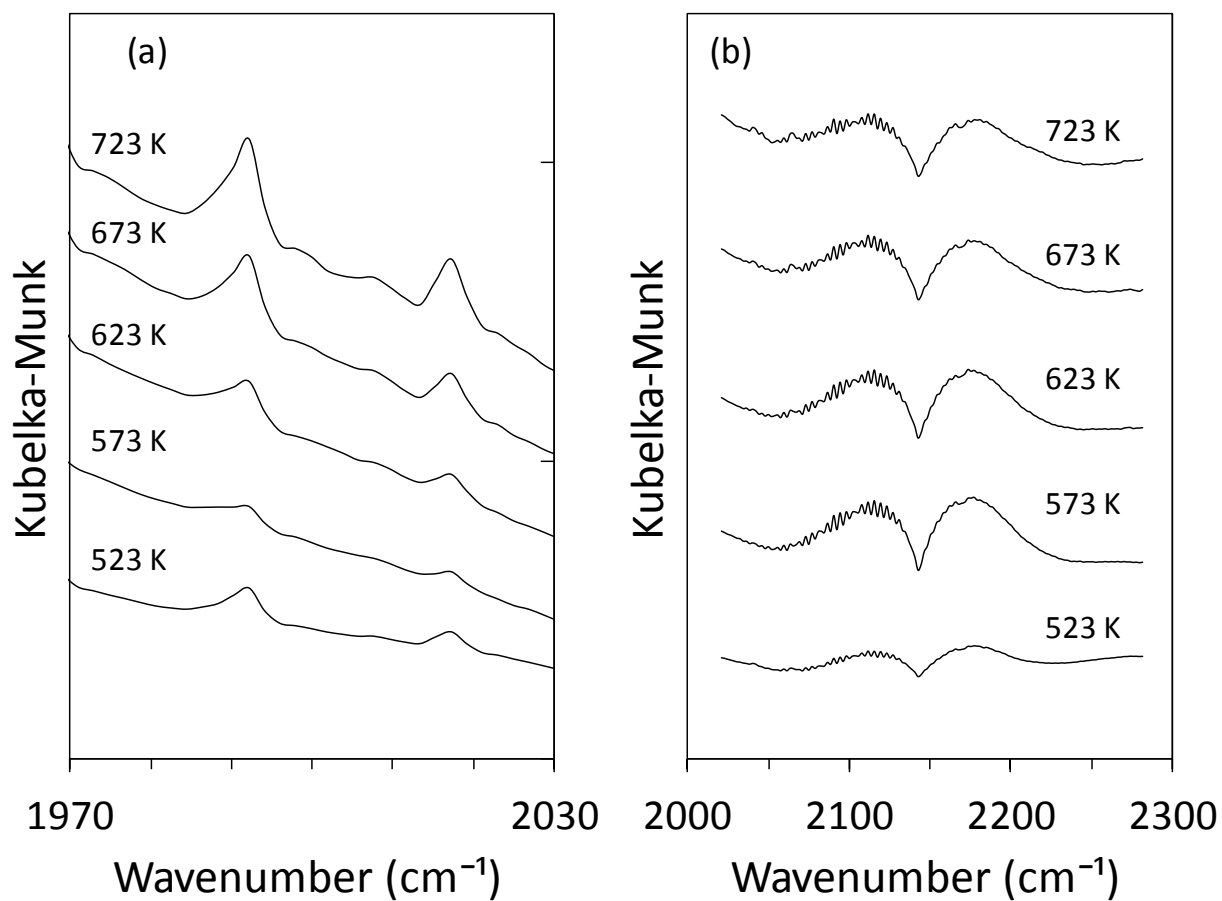


Figure 8. Detailed DRIFT spectra in the ranges of CO signals on Pd/Mg-Al surface as function of the temperature. Spectra focused on the area of (a) adsorbed CO; and (b) gas-phase free CO.

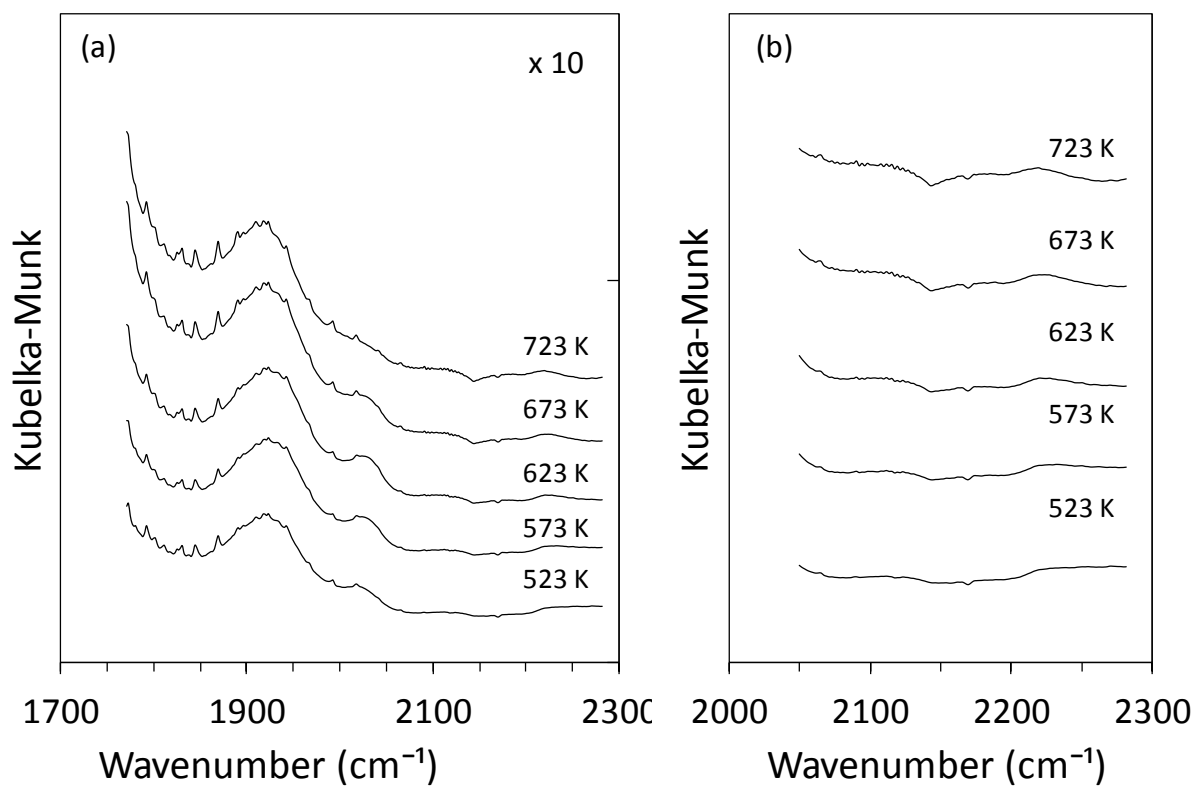


Figure 9. Detailed DRIFT spectra in the ranges of CO signals on Ru/Mg-Al surface as function of the temperature. Spectra focused on the area of (a) adsorbed CO; and (b) gas-phase free CO.

Table 1. Main results of the fresh catalysts characterization: morphological properties, density and distribution of the acid and basic sites, reduction temperature, and HRTEM results.

| Catalyst | Morphological properties | | | Acid sites ($\mu\text{mol g}^{-1}$), [T (K)] | | | Basic sites ($\mu\text{mol g}^{-1}$), [T (K)] | | | TPR reduction peak (K) | HR-TEM | |
|--------------|-------------------------------------|-----------------------|---------------------------------------------------|------------------------------------------------|---------------|--------------------|-------------------------------------------------|---------------|--------------------------|------------------------------|----------------------------|---------------------------------|
| | S ($\text{m}^2 \text{g}^{-1}$) | D _p (Å) | V _p ($\text{cm}^3 \text{g}^{-1}$) | weak | medium | Strong | weak | medium | strong | | Metal dispersion (%) | Crystallite diameter (nm) |
| Mg-Al | 226 | 135 | 0.7 | 11.3 [345, 370] | 12.5 [450] | 41.8 [630, 800] | 49.7 [340] | 71.7 [400] | 238.6 [630, 670, 800] | - | - | - |
| Pd | 215 | 45 | 0.4 | 2.6 [325, 357] | 3.3 [419] | 4.4 [523] | 83.6 [332, 379] | 56.7 [442] | 141.3 [625, 739] | 327 | 75.0 | 1.5 |
| Ru | 190 | 95 | 0.6 | 5.4 [333, 390] | 2.9 [466] | 1.7 [573] | 64.4 [327, 377] | 61.5 [449] | 21.2 [737, 812] | 585 | 76.0 | 1.7 |